Published in final edited form as:
Biochem J. ; 428(1): 33–45. doi:10.1042/BJ20100096.

Adaptor Protein 2 Regulates Receptor-Mediated Endocytosis and Cyst Formation in *Giardia lamblia*

Maria R. Rivero, **Cecilia V. Vranych**, **Mariano Bisbal**[*], **Belkys A. Maletto**[†], **Andrea S. Ropolo**, and **Maria C. Touz**[‡]

Instituto de Investigación Médica Mercedes y Martín Ferreyra. INIMEC – CONICET. Friuli 2434. Córdoba. Argentina

[†] Departamento de Bioquímica Clínica, CIBICI (CONICET), Facultad de Ciencias Químicas, Universidad Nacional de Córdoba, Córdoba, Argentina

Synopsis

The parasite *Giardia lamblia* possesses peripheral vacuoles (PVs) that function as both endosomes and lysosomes and are implicated in the adaptation, differentiation, and survival of the parasite in different environments. The mechanisms by which *Giardia* traffics essential proteins to these organelles and regulates their secretion have important implications in the control of parasite dissemination. In this study, we describe the participation of the heterotetrameric clathrin-adaptor protein gAP2 complex in lysosomal protein trafficking. A specific monoclonal antibody against the medium subunit (gμ2) of gAP2 showed localization of this complex to the PVs, cytoplasm, and plasma membrane in the growing trophozoites. gAP2 also colocalized with clathrin in the PVs, suggesting its involvement in endocytosis. Uptake experiments using standard molecules for the study of endocytosis revealed that gAP2 specifically participated in the endocytosis of LDL. Targeted downregulation of the gene encoding gμ2 in growing and encysting trophozoites resulted in a large decrease in the amount of cell growth and cyst wall formation, suggesting a distinct mechanism in which gAP2 is directly involved in both endocytosis and vesicular trafficking.

Keywords

Protozoa; adaptin; lysosome; encystation; endocytosis; LDL

Introduction

Giardia lamblia is a flagellated protozoan that inhabits the upper small intestine of its vertebrate hosts and is the most common cause of defined waterborne diarrhea in the United States and worldwide. In developing countries, there is a very high prevalence and incidence of infection, with recent data suggesting that long-term growth retardation can result from chronic giardiasis [1]. The clinical manifestations of giardiasis vary from an asymptomatic infection to an acute or chronic disease associated with diarrhea and malabsorption [1]. *Giardia* possesses a simple, two-stage life cycle. The infection initiates with the ingestion of the cyst form, which excysts in the upper small intestine of the host. The trophozoites replicate and colonize the intestinal surface, and some trophozoites encyst in the lower small intestine after sensing the stimulus for encystation [1,2]. Interestingly, during differentiation

[‡]Corresponding author: Maria Carolina Touz. Instituto de Investigación Médica Mercedes y Martín Ferreyra. INIMEC – CONICET. Friuli 2434. 5000. Córdoba. Argentina. Phone-fax: (54) (351) 468-1465/54-351-4695163. ctouz@immf.uncor.edu.
[*]Current address: Institut des Neurosciences Centre de Recherche Inserm U 836-UJF-CEA-CHU, Université Joseph Fourier, Faculté de Médecine, Cedex, France.

(encystation/excystation), trophozoites undergo important biochemical and morphological modifications involving the secretory machinery of the cell.

Giardia trophozoites lack a typical endosomal/lysosomal system. Instead, it possesses peripheral vacuoles (PVs), located underneath the plasma membrane of the trophozoites, which function as both endosomes and lysosomes [3]. Our previous studies into both vegetative and encysting parasites, have greatly contributed to a better understanding of protein trafficking toward the PVs in this important human pathogen [4–9]. However, several questions regarding this unique pathway remain unanswered. Because the PVs play an essential function in *Giardia* growth and differentiation, we believe that investigations into the role of the specific molecules involved in intracellular protein trafficking both to and from the PVs are necessary.

In mammalian cells, the role of clathrin and adaptor protein (AP) complexes in endosomal and lysosomal protein delivery is well established. For instance, it has been demonstrated that AP1 and AP3 are involved in protein trafficking toward the lysosomes, while AP2 participates in receptor-mediated endocytosis [10]. In *Giardia*, the lysosomal sorting pathway is not well defined. However, the presence of genes encoding a clathrin heavy chain as well as AP1 and AP2 complexes has been identified in the *Giardia* genome [11,12], supporting the hypothesis that AP1 and AP2 participate in protein transport to lysosome-like PVs in *Giardia*. No other adaptor complex proteins, such as AP3 and AP4 or the monomeric adaptors GGA, Hrs, or ARH [13], are represented in the *Giardia* genome.

We have previously demonstrated that gAP1 participates in lysosomal protein trafficking from a poorly defined sorting organelle to the PVs in *Giardia* [8]. However, the function of gAP2 remained unknown. Given the mechanisms present in more evolved cells, we hypothesize that gAP2 is the adaptor protein involved in vesicular trafficking from the plasma membrane to the PVs (the endocytic process). The heterotetrameric AP2 adaptor protein complex is composed of four subunits: two large chains (α and β2), one medium-sized chain (μ2), and one small chain (σ2) [10]. The APs have been described in different subcellular locations, where they may specifically function in cargo selection [14]. In this study, we functionally characterize the medium subunit of AP2 in *Giardia* (gμ2), which shares a strong structural identity with the mammalian counterpart that plays a vital role in the maintenance of the endocytic system. We generated a monoclonal antibody (mAb) against the gμ2 subunit to analyze the subcellular localization of gAP2, its relationship with clathrin, and its role during growth and encystation. Additionally, a double-stranded RNA strategy was used for g*μ2* protein knockdown experiments to study the role of gAP2 in receptor-dependent and -independent endocytic mechanisms and in *Giardia* survival. We observed that the receptor-mediated endocytosis of low-density lipoprotein (LDL) was impaired and that the production of cysts was drastically reduced in cells lacking gμ2. In this work, we describe the multifunctional role of gμ2 during different *Giardia* life stages, suggesting the participation of gAP2 in endocytosis and cyst formation, essential mechanisms for the parasite's survival.

Experimental

Ethics Statement

The animals (BALB/c mice) breed and maintain at the vivarium of the Instituto Mercedes &Martin Ferreyra (INIMEC-CONICET) have been inspected and approved by the Department of Animal Care (SENASA) from Argentina. Animal maintenance and care follow the general guidelines provided by The National Institute of Health of the United States of America.

Antibodies and other Reagents

The generation of the anti-gμ2 mAb specific for the gμ2 subunit of gAP2 is described below. The GiCLH polyclonal antibody specific for the *Giardia* clathrin heavy chain was a gift of A. Hehl [12]. The fluorescein-labelled anti-CWP1 mAb was obtained from Waterborne, Inc. Both BODIPY-labelled LDL and LysoTracker Red DND-99 were purchased from Molecular Probes-Invitrogen. The fluoronanogold-1.4nm-conjugated anti-mouse immunoglobulin G Fab fragment was obtained from Nanoprobes. The 20 kDa FITC-dextran and the FITC-transferrin were purchased from Sigma.

Giardia Cell Lines and Vectors

Trophozoites of the isolate WB, clone 1267 [15], were cultured in TYI-S-33 medium supplemented with 10% adult bovine serum and 0.5 mg/ml bovine bile, as previously described [16]. These trophozoites were used as hosts for the expression of the transgenic gene *ha-μ2* as non-transfected control. Briefly, the *Giardia μ2* gene was cloned into the pINDGtet tetracycline-inducible vector [17], and the protein was tagged with the HA epitope between amino acids 78 and 79, producing the pHAμ2tet vector. Trophozoite monolayers were induced to encyst by the method described by Boucher and Gillin [18]. For the uptake experiments, trophozoites were cultured in lipoprotein-deficient medium (TYI-S-33 medium supplemented with 10% human lipoprotein-deficient serum (Sigma) and 0.5 mg/ml bovine bile).

Purification of Peripheral Vacuoles

To purify PVs, *Giardia* trophozoites transfected with pESCP-HA (a PV protein marker) [7] and non-transfected trophozoites were harvested, homogenized, and resuspended in 1.0 ml of 250 mM sucrose containing the Complete Protease Inhibitor Cocktail (Roche). The lysates were then sonicated three times at 4°C (30 s, 20 A, in a VCX 130 Sonic Disruptor) and centrifuged at 1,000 × g for 10 min to remove unbroken cells and nuclei. The supernatant was then layered on a discontinuous sucrose gradient that was formed by layering 750 μl of 60, 55, 50, 45, 40, 35, 30, and 25% (w/w) sucrose into an SW 40 polyallomer centrifuge tube. The gradient was centrifuged for 18 h at 100,000 × g and fractionated from the top into 16 fractions (100 μl each). Proteins were precipitated by the addition of 10% TCA. To detect PV proteins, a 20 μl aliquot from each fraction was analyzed by dot-blotting using the anti-HA mAb to detect the ESCP-HA or 9B10 mAb for the surface protein, VSP9B10 (control) (Figure S1A). Fractions 7 to 12, containing purified PVs, were pooled and used for mouse immunization.

Generation of a Monoclonal Antibody Against gμ2

PV proteins (100 μg) were emulsified in TiterMax adjuvant (Sigma) and used to subcutaneously immunize BALB/c mice. Mice were boosted subcutaneously after 21 days with 200 μg of the same preparation and 20 days later, boosted again intravenously with 100 μg of the antigen suspended in PBS. Three days later, mice producing PV positive pAb (Figure S1B) were euthanized, and the spleen cells were fused to the NSO myeloma cell line (ECACC85110503). Antibody-secreting hybridomas were screened with indirect immunofluorescence and dot-blotting using non-encysting trophozoites and PV resident recombinant proteins, respectively. Five PV-specific mAbs were obtained, with one being specific for the gμ2 subunit (Figure S1C). We determined that the isotype of this anti-gμ2 mAb was IgG1. Briefly, the PV resident protein acid phosphatase (AcPh), clathrin heavy chain (CLH), Early Endosome Antigen 1 (EEA1), SNARE (Qa1), encystation-specific cysteine protease (ESCP), and the subunits of AP1 (β1, μ1, α1) and AP2 (β2, μ2, α2), were fused with GST by cloning into the pGex-4T-3. After small-scale protein expression and glutathione purification, the proteins were tested by dot-blotting using mAbs 2F5, 3H7, 8H1,

6A1, and 7A7. Cyst wall protein 2 (CWP2) fused with GST as well as GST alone were used as negative controls (Figure S1D).

Sequence Analysis

Homology searches were performed online with blastp at http://www.ncbi.nlm.nih.gov/blast/Blast.cgi. Swiss-Prot organism code GIALA (code); E (eukaryota); 5741(node): N = *G. lamblia*; Syn = *G. intestinalis*.

3D model prediction

3D modelling was performed with the Max Planck Institute Bioinformatics Toolkit, or HHPred (available at http://protevo.eb.tuebingen.mpg.de/toolkit/), which uses Modeller v7.7 for predictive modelling. MolMol [19] was used to create 3D images. The validation of the predicted 3D structures was performed with ANOLEA [20], Verify 3D [21], and MolProbity [22].

Immunofluorescence Assay (IFA)

Cells were washed with MPBS (1% growth medium in PBS, pH 7.4) and allowed to attach to the slides at 37°C. After fixation with 4% formaldehyde, the cells were blocked with PBS containing 10% normal goat serum and 0.1% Triton X-100. The cells were then incubated with the specific Abs in PBS containing 3% normal goat serum and 0.1% Triton X-100, followed by incubation with FITC-conjugated goat anti-mouse secondary antibody. For direct double staining, the anti-gμ2 mAb was labelled with Zenon Alexa Fluor 555 or 647 (final dilution of anti-gμ2 1:200) following the suggested protocol (Zenon Tricolor Mouse IgG_1 Labeling Kit, Molecular Probes) and added to the permeabilized cells together with the fluorescein-labelled anti-CWP1 mAb or LysoTracker. Finally, preparations were washed and mounted in Vectashield mounting medium. Fluorescence staining was visualized by using a spectral inverted confocal microscope (Olympus Fluoview 1000), using 100× oil immersion objectives (NA 1.32, zoom X). The fluorochromes were excited using an argon laser at 488 nm for FITC and a krypton laser at 568 nm for Texas Red 568. Detector slits were configured to minimize any crosstalk between the channels. Differential interference contrast images were collected simultaneously with the fluorescence images by the use of a transmitted light detector. Images were processed using FV10-ASW 1.4 Viewer and Adobe Photoshop 8.0 (Adobe Systems) software. The colocalization and deconvolution were performed using AutoDeblur&Autovisualize 9.3 software (Autoquant Imaging). To obtain colabelling of LysoTracker with anti-gμ2 mAb, trophozoites stained with LysoTracker were immediately fixed in 4% paraformaldehyde. The cells were subsequently stained with anti-gμ2 mAb (1:100) and Alexa Fluor 488-labelled goat anti-mouse secondary antibody (1:1000) (Invitrogen).

Immunoelectron microscopy (IEM)

Wild-type trophozoites were fixed *in situ* to preserve the cell organization using 2.5% glutaraldehyde in 0.1 M sodium cacodylate buffer, pH 7.1, and manipulated as previously described [7]. For immunostaining, the anti-gμ2 mAb (diluted 1:100 in a 3% globulin-free bovine serum albumin (BSA)-PBS solution) was added. The cells were then washed with PBS-BSA, and the fluoronanogold-1.4nm-conjugated anti-mouse antibody (diluted 1:40 in PBS-BSA with 0.01% saponin) was added. A second fixation was performed in 2% glutaraldehyde/4% formaldehyde in 100 mM cacodylate buffer, pH 7.4, for 1 h at 4°C. The samples were then incubated in a 1% osmium tetroxide post-fixative for 1 h at room temperature and dehydrated in increasing concentrations of acetone solutions. These samples were then embedded in Araldite (Electron Microscopy Science), and thin sections were cut using a Porter-Blum MT-2 and JEOL JUM-7 microtome. These sections were

mounted on 250 mesh nickel grids, and the grids were counterstained with aqueous uranyl acetate (1%) and lead citrate before being examined and photographed using a Zeiss LEO 906E electron microscope at the Electromicroscopy Center School of Medicine. Controls omitting the anti-gμ2 mAb, without treatment, or using a non-related antibody were processed simultaneously.

Immunoblot Analysis

Immunoblot assays were performed as previously reported [23]. 10 μg of total proteins from parasite lysates were incubated with sample buffer, boiled for 10 min, and separated in 10% Bis-Tris gels. Samples were transferred to nitrocellulose membranes, blocked with 5% skim milk and 0.1% Tween 20 in TBS, and then incubated with primary antibody diluted in the same buffer. After incubation with an enzyme-conjugated secondary antibody, proteins were visualized with the SuperSignal West Pico Chemiluminescent Substrate (Pierce) and autoradiography, or by using BCIP/NBT substrate (BioRad). Controls included the omission of the primary antibody, the use of an unrelated antibody, or assays using non-transfected cells.

gμ2 Downregulation

Previously, we developed a dsRNA vector for the inducible expression of double-stranded RNAs in *Giardia* (GenBank GU395185) [8] (Figure S2). This vector contains opposing *Giardia ran* promoters with tetracycline (Tet) operator elements and was designed for the insertion and double-stranded expression of PCR products. Additionally, it has a puromycin cassette under the control of the endogenous, non-regulated *gdh* promoter. To silence the *gμ2* gene, nucleotides 1–1000 from the 1305 nt of *μ2* were introduced into the dsRNA vector following PCR amplification of *gμ2* using the dsRNAμ2F (**a**): 5′-*gttggatccatgatcaaggcggtcattcttttggat*-3′ and dsRNAμ2R (**a′**): 5′-*ggtgcatgcccacctaatctgataagtccccgcgct*-3′ primers. The resulting pgμ2-dsRNA vector (10 μg) was used to transfect the *Giardia* clone WB1267 as described. After 48 h of tetracycline induction (10 μg/ml, final concentration), dsRNA production and *gμ2* depletion (by detection of the 305-3′ nt of *gμ2*) were confirmed by RT-PCR before performing analysis of cell growth, encystation, and uptake experiments.

Reverse transcriptase (RT)-PCR

Total RNA was isolated using the Trizol reagent (Invitrogen), and a second purification performed using the SV Total RNA Isolation System (Promega). The One-step RT-PCR Kit (Qiagen) was used for reverse transcription and PCR amplification. For semi-quantitative (sq) RT-PCR, total RNA was diluted serially from 20 ng to 0.2 ng per reaction in a final reaction volume of 50 μl, and RT-PCR was carried out following the manufacturer's instructions. For the RT-PCR shown in Figure 2C, the *atgatcaaggcggtcattcttttggat*/*acaggccgcgcaaagaacttcgtgcag* and the *atgtccactatgaggggtctcaagaa*/*taaaacgaaggtgcaactcagacgcc* oligonucleotide pairs for gμ2 and gα2, respectively, were used. For the RT-PCR shown in Figure 5C, an experiment using 10 ng of total RNA was shown as an example. For detection of gμ2 sense mRNA from pgμ2-dsRNA, the **a** + **b** (*gttggatccatgatcaaggcggtcattcttttggat*/*ccctgatcctctagaatttcaaaattaaagctaaa)* primers were used. To detect the gμ2 antisense mRNA from pgμ2-dsRNA, the **b** primer was added in the reverse transcription step, followed by the addition of the primer for PCR amplification. To determine the level of endogenous *gμ2* sense mRNA, the **c** + **d** (*accgccatcgaatcactcgggaagtgc*/*ggtgcatgcgacgtctgagacgttcgagggcatagg*) primer pair was used (Figure 5A–C). A DNA contamination control was performed by adding the same primers at the PCR step of the RT-PCR reaction (not shown). To control for specificity and the amounts of RNA loaded into the reaction, the expression levels of the constitutively expressed glutamate dehydrogenase enzyme (GDH) and *gμ1* were determined by RT-PCR

using previously described primers GDHf/GDHr and *gμ1*-NcoI/*gμ1*-EcoRI, respectively [23]. Aliquots (5 μl) of the RT-PCR reaction were separated on a 1.2% agarose gel in TAE (E-Gel, Invitrogen) prestained with ethidium bromide. Amplification products were directly quantified by densitometric scanning of the fluorescence intensity under UV light using EagleSight software for image acquisition, documentation, and analysis (Stratagene). These assays were performed four times and statistically analyzed.

Slot-Blot Assay

The assay was performed as described [8]. Membranes were first hybridized with antisense probes specific for the last 305 base pairs of *gμ2* gene and then stripped and probed by using an antisense oligonucleotide specific for *gdh* or *gμ1* as a control for RNA input and specificity, respectively.

Growth curves

For the growth curve, tubes containing 7 ml of growth medium without puromycin were inoculated with 10^4 trophozoites from wild-type, gμ1-dsRNA [8], or F2 transgenic gμ2-dsRNA logarithmic phase cultures. Tetracycline (10 μg/ml, final concentration) was added to wild-type, gμ1-dsRNA, or transgenic gμ2-dsRNA to test the effect of Tet and gμ(1–2) depletion in trophozoite growth. Every 12 h, the medium was decanted and the tubes were chilled on ice for 20 min to detach adherent living trophozoites. The number of viable cells was determined by counting on a haemocytometer. For growth recovery experiments, 10^4 wild-type trophozoites were grown in lipoprotein-deficient growth medium and growth recovery measured at 2, 8, 16, 24, and 48 h of cultivation after addition of LDL or chylomicrons (100 μg/ml, Athens Research & Technology). The medium was decanted and the tubes chilled on ice for 20 min to detach adherent living trophozoites. The number of viable cells was determined by counting on a haemocytometer.

Flow cytometry Analysis

For the evaluation of the completion of the encystation process, the trophozoites were grown to a monolayer in pre-encysting media and induced to encyst as described below. To induce dsRNA, 10 μg/ml of Tet was added to the preencysting and encysting media without addition of puromycin. After 48 h, cysts were collected, fixed in 4% paraformaldehyde, and stained with FITC-labelled anti-CWP1. Cysts were then washed and analyzed on a Cytoron Absolute Cytometer (Ortho Diagnostic System). Data were analyzed using the WinMDI version 2.8 software (http://facs.scripps.edu).

Uptake experiments

For the receptor-mediated endocytosis assays, wild-type *Giardia* trophozoites were incubated for up to 2 h at 4°C, which normally inhibits endocytosis, in labelling media containing BODIPY-LDL or FITC-dextran, washed and then transferred to 37°C for 2 h for endocytosis recovery. The LDL binding assays were performed by growing wild-type cells in the absence of LDL, in the presence of a 10-fold excess of unlabelled LDL, 100 μg/ml of chylomicrons, or 500 μg/ml of HDL (Sigma) before the addition of BODIPY-LDL for 45 minutes, 1, 2, and 6 h at 37°C. Cells were then collected by centrifugation at 2,500 × g for 10 min at 4°C, washed with cold mPBS, and observed by epifluorescence microscopy. To analyze the role of gAP2 in endocytosis, either 20 kDa FITC-dextran or BODIPY-LDL was used as an endocytic marker to study fluid phase or receptor-mediated endocytosis mechanisms, respectively. Briefly, trophozoites transfected with the pgμ2dsRNA vector were cultured for two days in the presence of 10 μg/ml of tetracycline to induce μ2-dsRNA expression. The uptake experiments were performed by exchanging the growth medium for labelling buffer (50 mM glucose, 10 mM cysteine, 2 mM ascorbic acid in PBS, pH 7.1)

containing either 2 mg/ml FITC-dextran or 7.5 μg of BODIPY-labelled LDL. After 6 h at 37°C, the trophozoites were visualized by fluorescence microscopy. Controls for this experiment included the addition of FITC-dextran or BODIPY-LDL to wild-type trophozoites and non-tetracycline induced cells.

Statistics

Descriptive statistics for −ds and +ds cells growth curves included the calculation of the means and standard deviations of the control and experimental groups. A comparison of the means was performed using the Independent-Samples Student's t-test from the SSPS Statistic program. $p \leq 0.05$ was considered significant. For growth curves after chylomicron addition, a single-factor analysis of variance (ANOVA) and the Dunnett's multiple comparison tests were used. $p < 0.05$ was considered significant.

Results

Characterization of *Giardia* Adaptor protein 2

The completion of the sequencing of the *Giardia* WB genome (GGD: http://www.giardiadb.org/giardiadb/) confirmed that there are only two heterotetrameric adaptor protein complexes, gAP1 and gAP2, present in this parasite. The analysis of the secondary sequence homology of the medium subunit of gAP2 (gμ2) (GDB: GL8917) revealed that this subunit possesses 32% identity and 55% similarity with the same subunit from rat, mouse, and human (Figure S3A). In addition, we used the secondary structure information, along with residue-residue contact information, for tertiary structure prediction using the hidden Markov models (HMMs) (Figure S3B) [24] and MODELLER (see Materials and Methods) [25]. We observed that the validated 3D structure was highly homologous to the crystal structure of μ2 from rat. More important, the cargo binding site residues, Asp^{173} and Trp^{420}, were similarly exposed in both subunits, suggesting that gμ2 may have an equivalent role to the subunit in rat in endocytosis (Figure 1).

In previous experiments, we found that the HA-tagged gμ2 localized mainly to the PVs (Figure S1F). This result prompted us to develop mAbs against these purified organelles to further characterize gμ2 (see Experimental and Figure S1A–E). Five hybridomas showed reactivity toward the PVs by indirect immunofluorescence (Figure S1C). The specificity of these antibodies was further analyzed by probing GST-tagged PV resident proteins, acid phosphatase, clathrin, early endosome antigen 1, Qa-SNARE, encystation-specific cysteine protease, and the four subunits of AP1 and AP2, in dot-blotting [9, 12, 26, 27] (Figure S1D). This assay revealed that one of the hybridomas produced the mAb 2F5, with affinity for GST-μ2 (Figure S1D). Immunoblot analysis using GST-μ2 purified protein and an homogenate of WB1267 trophozoites showed that the anti-μ2 mAb (2F5) was able to recognize both the recombinant 80 kDa GST-gμ2 protein and the predicted 50 kDa native gμ2 under reducing conditions (Figure 2A). Moreover, this mAb was able to immunoprecipitate the HA-gμ2 fusion protein expressed in *Giardia* trophozoites and also recognized HA-gμ2 in transgenic trophozoites by IFA (Figure S1E–F). Because we established the specificity of the mAb 2F5 against the native gμ2 subunit, we used this antibody to functionally characterize the gAP2 complex. Analysis of protein expression dynamics by immunoblotting for gμ2 in trophozoites vs. 24 h-encysting cells showed no essential differences between the two stages (Figure 2B). Observation of CWP1 expression at 24 h post induction was used as a positive control for encystation (Figure 2B). In the same way, a semi-quantitative RT-PCR assay of *gμ2* and *gα2* mRNAs revealed no changes in transcript levels during encystation compared with *cwp1* (Figure 2C), confirming a previous report that showed that *gβ2* transcription was unaltered during stage conversion [12]. The mRNA levels of the encysting cells expressed *cwp1* and the constitutively expressed *gdh*

(not shown), were tested as positive controls for encystation and RNA concentration, respectively.

Giardia medium subunit of AP2 (gμ2) localized to lysosome-like peripheral vacuoles and the plasma membrane

By IFA and confocal laser scanning microscopy using the anti-μ2 mAb, we determined that the native gμ2 was mainly localized underneath the plasma membrane (Figure 3A). To reveal the localization of AP2, we used LysoTracker Red, which is able to partition into acidic organelles (e.g., lysosomes and late endosomes) of living cells and also specifically label PVs [7]. We found that LysoTracker and gμ2 colocalized in the PVs (Figure 3B). Interesting, some cells depicted staining with LysoTracker and gμ2 in a central bare zone with unknown functions.

Confirmation of gμ2 localization to the PVs was obtained using immunoelectron microscopy of WB1267 trophozoites. A typical electron micrograph of a *Giardia* trophozoite showed the presence of both nuclei and the distribution of the PVs beneath the plasma membrane (Figure 4A, a). We consistent labelled these structures, with some specific labelling on the inner side of the plasma membrane, by treating the cells with anti-gμ2 mAb and the 1.4nm gold-labelled secondary antibody (Figure 4A, b–f). No obvious gold labelling was observed in the bare zone in the trophozoites analyzed (not shown). Labelling was observed neither in untreated control nor in cells treated with secondary antibody alone (Figure 4A, g–h). Taking into account the localization of gμ2 and the known function of AP2 in eukaryotes, we hypothesised that gAP2 is part of the coated vesicles that are responsible for the recruitment of clathrin molecules to form clathrin-coated vesicles (CCV) during endocytosis. In fact, confocal immunofluorescence microscopy of trophozoites showed that the localization of gμ2 overlapped with the *Giardia* clathrin heavy chain (GiCLH) in the PV area (Figure 4B). Thus, it is highly probable that gμ2 has functional similarities to the mammalian μ2 subunit, specifically acting in concert with receptors and clathrin to mediate endocytosis.

Depletion of μ-AP2

Gene knockout is difficult in *Giardia* due to the polyploid nature of its genome [1]. An alternative approach, which has gained prominence in recent years, is RNAi, post-transcriptional gene silencing by the expression of homologous double-stranded RNA (dsRNA) [28]. An adaptation of this technique, producing long dsRNA fragments, has been previously used to functionally downregulate *Giardia* gene expression during growth and encystation [8,29]. Therefore, to silence the *gμ2* gene, nucleotides 1–1000 from the *gμ2* ORF were cloned into a dsRNA expression vector (Figure S2), yielding the pgμ2-dsRNA (Figure 5A). After WB1267 trophozoite transfection and selection, the double-stranded RNA was induced by the addition of 10 μg/ml of tetracycline. Forty-eight hours later, the effect of the dsRNA on *gμ2* expression was analyzed by RT-PCR using total RNA from trophozoites expressing *gμ2*-dsRNA (+ds) or non-expressing *gμ2*-dsRNA (−ds). As seen in Figure 5B, the exogenous 5′ *gμ2* sense and antisense mRNA from the pgμ2-dsRNA vector was confirmed by using a combination of the *a* + *b* primers (see Experimental), while the 3′ endogenous *gμ2* sense mRNA was exclusively verified using the *c* + *d* primers (Figure 5B). Densitometric analysis of the semi-quantitative RT-PCR showed that equal levels of sense and antisense gμ2 RNA from the pgμ2-dsRNA were present in +ds but not in −ds or wild-type cells (Figure 5C). Furthermore, a significant reduction of the endogenous *gμ2* mRNA was observed in +ds trophozoites compared with −ds or wild-type cells when the 3′endogenous 305 nt segment was tested, showing that the production of *gμ2*-dsRNA successfully diminished the transcript levels of *gμ2* mRNA (Figure 5C). The mRNA levels of the housekeeping gene, *gdh* (Figure 5C), and *gμ1* (not shown) did not demonstrate

significant variation between wild-type, −ds, and +ds trophozoites. The same results were obtained by slot-blotting; only *gμ2* mRNA was reduced in +ds trophozoites while *gdh* and the *gμ2*-homologous *gμ1* mRNA remained (Figure 5D). These results validate the previous results that showed that the production of dsRNA does not appear to affect the mRNA level non-specifically [8,29]. Several clones from gμ2-dsRNA transgenic trophozoites were analyzed by RT-PCR over time. We observed that the clone F2 was the one that produced the most significant reduction of gμ2 endogenous mRNA expression at 48 h. Consequently, F2 gμ2-dsRNA cells were grown and employed for further analysis.

The inhibition of gμ2 protein expression was tested by direct IFA, which showed slight labelling of +ds cells (Figure 5E, gμ2, bottom panel) compared with −ds ones (Figure 5E, gμ2, top panel) using the Alexa Fluor 647-labelled anti-μ2 mAb. Due to the fact that gμ2 disruption may affect the normal morphology and function of the PVs (as acidic organelles), we stained −ds and +ds trophozoites with LysoTracker. The typical labelling pattern of these organelles underneath the plasma membrane was observed in both −ds and +ds cells, demonstrating that the PVs were not affected (Figure 5E, LysoTracker). Immunoblotting using anti-gμ2 mAb showed that the 50 kDa band corresponding to gμ2 was almost undetectable in +ds transgenic trophozoite homogenates, compared with wild-type and −ds cells as well as tubulin (loading control) (Figure 5F). Taken together, the results above demonstrate that the expression of gμ2 was significantly reduced in +ds trophozoites compared with −ds trophozoites.

gμ2 depletion impairs *Giardia* growth

It is well known that endocytosis allows the uptake of nutrients in many cells, including protozoan parasites. Because gAP2 may be involved in the incorporation of nutrients that are essential for *Giardia*, we analyzed the effect of gμ2 depletion on cell growth. To characterize the growth pattern of +ds cells compared with −ds and wild-type control cells, a growth curve was established. Relative to −ds, cell growth in +ds was three-fold lower at 48 h and approximately seven-fold lower at 60 hours, with this being the maximum difference (Figure S4). Over 96 hours, modifications in the cell shape and aggregation but not vesiculation occurred in +ds cells, and ultimately, cell death followed. However, there was a significant window of time in which the μ2-depleted phenotype could be analyzed in otherwise healthy cells. The addition of tetracycline to wild-type cells (WB1267+tet) or μ1-depleted cells (μ1+tet) [8] resulted in a minor (1.2 times) decrease in cell growth at 48 h compared with cell cultures without tetracycline (WB1267 and μ1) (Figure S4). In these controls, no cell death was observed after 96 h of cultivation. Thus, the striking phenotype observed in +ds trophozoites can be attributed to the effective reduction of the *gμ2* mRNA and protein levels shown above. The lower influence of tetracycline on cell growth at 48 h in wild-type cells prompted us to employ this time point for Tet-induced cultures in the uptake and differentiation experiments.

Specialized capture and internalization of LDL in living trophozoites

Molecules such us horseradish peroxidase (HRP) and dextran are internalized by fluid-phase endocytosis, a non-specialized process unable to guarantee a strictly specific effect. In contrast, the most specific mode of uptake of macromolecules is receptor-mediated endocytosis, whereby plasma membrane proteins bind a ligand (e.g., albumin, transferrin, or low-density lipoprotein (LDL)) and adaptor proteins (e.g., AP2, ARH, or Dab), causing the clustering of these molecules in clathrin-coated pits and resulting in accelerated internalization. It was shown that gold-labelled HRP, albumin, transferrin, and LDL were endocytosed by *Giardia* and only seen in the PVs [30]. It was also demonstrated that LDL supported *Giardia* growth in culture medium and suggested that this molecule was internalized by a cell surface receptor [5]. To investigate whether LDL is indeed

endocytosed by a protein receptor, classic experiments using BODIPY-LDL were performed by reproducing, in part, previous experiments [5]. Wild-type trophozoites were incubated for up to 2 h at 4°C (a situation that inhibits endocytosis) in the labelling medium containing BODIPY-LDL. Following this incubation, the LDL was associated with the plasma membrane but not internalized (Figure S5A, 4°C). After washing, LDL endocytosis was then restarted by returning the cells back to 37°C for another two hours. After internalisation during endocytosis recovery, LDL was delivered to the PVs (Figure S5A, 37°C). In this experiment, it was also possible to observe that LDL formed patches on the surface before internalization, suggesting the presence of a receptor at the cell surface. Similar experiments using FITC-dextran or FITC-transferrin did not show association with the membrane at 4°C (not shown).

To examine whether LDL was bound to a particular surface protein, we evaluated the time course of BODIPY-LDL uptake with the trophozoites first challenged with different lipoproteins. Wild-type trophozoites were grown on lipoprotein-deficient medium (see Experimental) and then incubated with the unlabelled lipoprotein LDL, high-density lipoprotein (HDL), or chylomicrons before addition of BODIPY-LDL. The resulting uptake of BODIPY-LDL was then compared with the internalization of BODIPY-LDL by control cells lacking the initial treatment with unlabelled lipoproteins. In control cells, we observed that the uptake of BODIPY-LDL increased over time with maximum accumulation occurring at two hours (Figure 6, −LDL). Observing the cells longer than two hours also showed labelling of the nuclear envelope (Figure 6, −LDL, 6h). On the other hand, labelling by BODIPY-LDL was reduced in the presence of a 10-fold excess of unlabelled LDL (Figure 6, +LDL) but not with HDL (not shown). Interestingly, BODIPY-LDL uptake was completely inhibited when the trophozoites had been previously incubated with chylomicrons (Figure 6, +Chylomicrons).

Because we observed that chylomicrons were able to inhibit LDL uptake, we hypothesized that both lipoproteins are used by *Giardia* trophozoites to acquire cholesterol either *in vivo* or *in vitro*. We observed that the growth of trophozoites in lipoprotein-deficient medium was significantly lower than in medium containing LDL. Interestingly, addition of chylomicrons to trophozoites growing in lipoprotein-deficient medium restored the cell growth to normal levels, suggesting that the trophozoites were able to utilize this lipoprotein as a nutrient resource (Figure S6).

gμ2 is involved in receptor-mediated endocytosis in *Giardia*

To address whether the internalization of cholesterol from LDL occurs via a regulated, AP2-dependent pathway, we tested the uptake of BODIPY-LDL in −ds and +ds trophozoites and used FITC-dextran as a control for fluid-phase endocytosis [31]. Trophozoites were visualized six hours after addition of BODIPY-LDL or FITC-dextran to −ds and +ds cells and incubation at 37°C. Confocal microscopy revealed that both BODIPY-LDL and FITC-dextran were endocytosed and localized to the PVs in −ds cells (Figure 7, left panels and Figure S5B). On the other hand, in +ds cells, the LDL was not internalized but rather, was retained on the surface (including the flagella), although dextran was delivered to the PVs (Figure 7, right panels and Figure S5B). Because BODIPY-FL-LDL fluoresces slightly in the red region, we were unable to use LysoTracker (red) in the same cells to colocalize both molecules in the PVs. However, an overlay of the differential interference contrast (DIC) image with BODIPY-LDL or FITC-dextran accumulations in −ds cells showed a similar pattern to the one shown for LysoTracker and gμ2 (Figure 3). Uptake experiments using FITC-transferrin showed that this molecule was equally endocytosed in −ds and +ds cells (not shown). All together, the information provided by these results suggests that AP2 specifically participates in the endocytosis of LDL, most probably by a receptor-mediated mechanism.

The presence of gμ2 is decisive during cyst wall formation

The differentiation of *Giardia* into the cyst form (encystation) allows the parasite to survive in an unfavourable environment, thereby increasing the likelihood of infection of a new host. The process of encystation can be divided into four distinct phases: i) the detection of the stimulus that triggers the expression of specific genes, ii) the synthesis and transport of the electrodense cyst wall components (CWPs) into encystation-specific vesicles (ESVs), iii) the assembly of the extracellular cyst wall (CW), and iv) nuclear division and DNA replication [1]. Immunoelectron microscopy of encysting trophozoites showed that at the end of the phase (ii) of encystation, the PVs containing gμ2 enfolded the ESVs (Figure 8A, left panel). This close proximity might allow an interchange of material between both organelles, as has been observed during the CWP maturation process [7,32–34]. During phase (iii), gμ2 was observed at the plasma membrane and remained on the inner side of membrane, at the point where the CWPs are released to form the filamentous cyst wall (Figure 8A, right panel).

To further analyze the role of gAP2 during encystation, −ds and +ds cells were induced to encyst in the absence or presence of tetracycline, respectively, and analyzed by microscopy and flow cytometry using the anti-CWP1 mAb (that detects cyst wall protein 1 in mature cysts). Approximately 4–8% of total WB1267 wild-type trophozoites were previously found to differentiate into cysts after 48 h in encysting medium [35]. IFA and microscopic analysis of cysts stained with the fluorescein-labelled CWP1 mAb revealed almost a complete absence of cysts in +ds cells compared with −ds ones (Figure 8B). Moreover, a quantitative analysis of cysts by flow cytometry showed that the silencing of gμ2 drastically reduced the number of cysts (by approximately 50 times) compared with the wild-type (not shown) or −ds cells (Figure 8C).

Discussion

This work provides a number of new observations that have significant mechanistic implications for adaptor-mediated endocytosis in *Giardia lamblia*. We found that *Giardia* utilizes adaptor protein complex 2 (gAP2) to internalize LDL, probably by receptor mediated endocytosis. Interestingly, we found that the gAP2 complex specifically localized to the inner side of the plasma membrane and to the PVs, similar to the previously described distribution of clathrin [36]. Gaechter *et al.*, recently demonstrated that the *Giardia* dynamin-related protein (GiDRP) also localized to the PVs with clathrin. Moreover, the expression of a mutant DRP, which had a reduced affinity for GTP and GDP, not only blocked the internalization of surface proteins as expected, but also resulted in enlarged PVs, indicative of blocked vesicular fission in these organelles [31]. This finding, together with the work presented here, raises the question of whether these vacuoles may act as sorting organelles by selectively delivering proteins to the plasma membrane and/or returning others back to the ER exit site.

RNA interference (RNAi) is defined as the mechanism through which gene-specific, double-stranded RNA (dsRNA) triggers degradation of homologous transcripts. Information extracted from available databases predicted that *Entamoeba histolytica* and *Giardia* have an RNAi pathway, supporting the view that gene silencing by dsRNA might occur in these parasites [37]. Indeed, recent reports have described the existence and function of the enzymes involved in the RNAi process [38,39], indicating that an RNAi mechanism may be involved in the control of endogenous genes rather than being a tool to downregulate foreign gene expression [38,39]. Nevertheless, downregulation of gene expression by “long” dsRNA has previously been described [9,38]. We used this approach to functionally analyze the role of the gAP2. We found that 48 h after 1,000 nt *gμ2*-dsRNA production, there was almost no expression of the endogenous gμ2. If the *gμ2*-dsRNA expression had indeed been decreased via an RNAi mechanism, we would have expected to see the processing of this dsRNA into

nucleotide siRNAs by the RNase, *Giardia* Dicer [38]. However, no degradation to small RNAs was detected, suggesting that the reduction in gμ2 expression by this technique was unlikely to have been due to an RNAi mechanism (Rivero *et al*. submitted).

Because the gμ2-depleted trophozoites did not show any significant changes in the number or morphology of their PVs compared with wild-type trophozoites, we conclude that the gAP2 complex does not maintain the structure of the PVs. Nevertheless, these transgenic cells grew significantly slower than the wild-type trophozoites and showed considerable signs of deterioration over long-term *in vitro* culturing. One explanation for this phenomenon could be that the μ2-depleted trophozoites are unable to successfully endocytose lipoproteins. Indeed, low-density lipoprotein (LDL) was shown to be essential for long-term growth *in vitro* [5,40]. In this study, we confirmed that LDL was retained at the plasma membrane before endocytosis and that this binding was likely to a particular protein because LDL but not HDL bound. In *in vivo* experiments, we observed that BODIPY-LDL localized to the PVs following endocytosis but was also observed around the nuclei in long-term tracking experiments. This finding is in agreement with the observation of Abodeel *et al*. that suggested that the endosome compartment in *Giardia* lies adjacent to the tubulovesicular network that extends to the perinuclear cisternae [41].

Although there is no LDL-receptor (LDLR) homologue in the *Giardia* genome, the data suggest that LDL is internalized via binding to a receptor protein. In this sense, in a GGD survey, we identified a protein that shares the lipoprotein-binding domain with LRP1 and LRP1b (Lipoprotein Receptor-related Protein), which is a member of the LDLR family [42,43] (Rivero *et al*. unpublished results). *Giardia* is unable to synthesize cholesterol *de novo* and might obtain this compound from the intestinal milieu or from the growth medium supplemented with serum. It is possible that, *in vivo*, the *Giardia* LRP-like receptor binds to chylomicrons present in the intestine via their apolipoprotein-B48 because several studies have shown the importance of LRP in the uptake of apo-B48-containing lipoproteins [44,45]. We observed that the presence of chylomicrons, but not the apoAI-containing HDL, inhibited the uptake of BODIPY-LDL, suggesting that LDL and chylomicrons bind to a surface protein that is likely able to recognize both apoB-containing lipoproteins. Furthermore, the rescue of the trophozoite growth rate after addition of chylomicrons supports the idea that the parasite is able to obtain cholesterol from this lipoprotein *in vivo*. Because the trophozoites normally thrive in an environment where they never come in contact with LDL, it is possible that the binding of LDL may represent an adaptation of the parasite to the culture medium. Ongoing investigations to verify the interaction of gLRP with apoB and gAP2 should lead to a better understanding of the function of cholesterol endocytosis in *Giardia*. Interestingly, our experiments using FITC-transferrin indicate that this molecule is not endocytosed in a receptor-binding manner and suggests that in the absence of a transferrin receptor homologous protein, transferrin is endocytosed by fluid phase endocytosis in Giardia.

Experiments using gμ2-depleted cells demonstrated that gAP2 participates in the endocytosis of LDL but not in the endocytosis of dextran. Additionally, we analysed whether clathrin was also involved in LDL endocytosis by performing potassium depletion experiments [46] using a previously described protocol [47]. Although LDL internalization was inhibited, the potassium depletion drastically altered the cellular morphology and made the analysis difficult (data not shown). Nevertheless, from the results presented here, we can conclude that the LDL binds to a receptor on the plasma membrane, thereby allowing the internalization of cholesterol in a gAP2-dependent manner.

Encystation of *Giardia* involves the formation of large encystation-specific secretory vesicles ESVs, which transport stage-specific proteins to the nascent cyst wall. During the

last decade, several groups have studied the development of ESVs and whether these vesicles experience a maturation process [32,48,49]. Nevertheless, no clear results have been obtained about the process of ESV material release. In addition, several authors have suggested that the PVs might be involved in the encystation [5,8,9,30,31,32]. It has been proposed that ESVs are broken up and dispersed into small vesicles targeted for the plasma membrane [31,48]. Moreover, electron microphotographs have shown an intimate contact between ESVs and PVs underneath the encysting trophozoite plasma membrane [7,32,49]. It was also reported that ESVs were surrounded by PVs [49] and that an exchange of material occurred among them [4,7]. It is therefore possible that fusion of these two organelles or traffic between them may take place during cyst wall formation. By immunoelectron microscopy, we found that gAP2 was present near the ESVs as well as in the PVs. Moreover, we observed that cyst production was drastically reduced in gμ2 knockdown trophozoites. In addition to having a role in endocytosis during *Giardia* growth, these results suggest a significant role of gAP2 in cyst wall formation during encystation. It was recently shown that cyst production was abolished when a GiDRP mutant was overexpressed without GiDRP recruitment to the ESVs, and this resulted in the abolition of small, CWP-containing vesicle formation [31]. Unfortunately, no information about the localization of clathrin was reported in these dominant-negative cells. Further analysis of the cooperative function of gAP2, GiDRP, and clathrin is necessary to provide conclusive information about the ultimate fate of ESVs at the end of the encystation.

It has been suggested that early cells evolved mechanisms to take up extracellular macromolecules (pinocytosis) and to secrete digestive enzymes directly into an endocytic vacuole that contained the appropriate nutrient pumps (the lysosome progenitor hypothesis) [50]. However, the molecular mechanisms underlying endocytosis have diversified considerably since their early evolutionary beginnings. In higher eukaryotes, distinct endocytic pathways are tightly regulated to control all aspects of intracellular communication. Conversely, in *Giardia*, the peripheral vacuoles function as a single endosomal/lysosomal organelle [3,7,8]. Furthermore, the machinery involved in the delivery of lysosomal proteins in this parasite also seems to be very simple. It is possible that this relatively straightforward lysosomal sorting and delivery system of *Giardia* might reflect the ancient nature of this parasite [51]. However, some of the particular cellular characteristics of *Giardia* are probably a result of the secondary loss of complex cell structures as a consequence of its parasitic lifestyle, rather than the primitive simplicity suggested for early diverging protists [4,52]. In either case, *Giardia* is a useful system to study not only the evolution of the secretory pathway in eukaryotes, but also to investigate ‘why’ and ‘how’ an organism may have lost some essential subcellular organelles while maintaining the minimal machinery necessary for fundamental cellular functions after becoming a parasite.

Supplementary Material

Refer to Web version on PubMed Central for supplementary material.

Acknowledgments

The project was supported by Grant Number R01TW00724 from the Fogarty International Center. The content is solely the responsibility of the authors and does not necessary represent the official views of the Fogarty International Center or the National Institutes of Health. This research was also supported in part by the Agencia Nacional para la Promoción de la Ciencia y Tecnología (FONCyT), and the National Council for Sciences and Technology (CONICET).

Abbreviations

PVs	peripheral vacuoles
AP	adaptor protein
mAb	monoclonal antibody
GST	glutathione S-transferase
FITC	fluorescein isothiocyanate
Tet	tetracycline
GDH	glutamate dehydrogenase enzyme
CCV	clathrin-coated vesicles
DIC	differential interference contrast
CWP	cyst wall protein
ESVs	encystation-specific vesicles
RNAi	RNA interference

References

1. Adam RD. Biology of Giardia lamblia. Clin Microbiol Rev. 2001; 14:447–475. [PubMed: 11432808]
2. Lujan HD, Diamond LS. Cholesterol requirement and metabolism in Entamoeba histolytica. Arch Med Res. 1997; 28(Spec No, 96–97)
3. Lanfredi-Rangel A, Attias M, de Carvalho TM, Kattenbach WM, De Souza W. The peripheral vesicles of trophozoites of the primitive protozoan Giardia lamblia may correspond to early and late endosomes and to lysosomes. J Struct Biol. 1998; 123:225–235. [PubMed: 9878577]
4. Lujan HD, Touz MC. Protein trafficking in Giardia lamblia. Cell Microbiol. 2003; 5:427–434. [PubMed: 12814433]
5. Lujan HD, Mowatt MR, Nash TE. Lipid requirements and lipid uptake by Giardia lamblia trophozoites in culture. J Eukaryot Microbiol. 1996; 43:237–242. [PubMed: 8640194]
6. Lujan HD, Mowatt MR, Conrad JT, Bowers B, Nash TE. Identification of a novel Giardia lamblia cyst wall protein with leucine-rich repeats. Implications for secretory granule formation and protein assembly into the cyst wall. J Biol Chem. 1995; 270:29307–29313. [PubMed: 7493963]
7. Touz MC, Lujan HD, Hayes SF, Nash TE. Sorting of encystation-specific cysteine protease to lysosome-like peripheral vacuoles in Giardia lamblia requires a conserved tyrosine-based motif. J Biol Chem. 2003; 278:6420–6426. [PubMed: 12466276]
8. Touz MC, Kulakova L, Nash TE. Adaptor protein complex 1 mediates the transport of lysosomal proteins from a Golgi-like organelle to peripheral vacuoles in the primitive eukaryote Giardia lamblia. Mol Biol Cell. 2004; 15:3053–3060. [PubMed: 15107467]
9. Touz MC, Nores MJ, Slavin I, Carmona C, Conrad JT, Mowatt MR, Nash TE, Coronel CE, Lujan HD. The activity of a developmentally regulated cysteine proteinase is required for cyst wall formation in the primitive eukaryote Giardia lamblia. J Biol Chem. 2002; 277:8474–8481. [PubMed: 11773053]
10. Bonifacino JS, Traub LM. Signals for sorting of transmembrane proteins to endosomes and lysosomes. Annu Rev Biochem. 2003; 72:395–447. [PubMed: 12651740]
11. Morrison HG, McArthur AG, Gillin FD, Aley SB, Adam RD, Olsen GJ, Best AA, Cande WZ, Chen F, Cipriano MJ, Davids BJ, Dawson SC, Elmendorf HG, Hehl AB, Holder ME, Huse SM, Kim UU, Lasek-Nesselquist E, Manning G, Nigam A, Nixon JE, Palm D, Passamaneck NE, Prabhu A, Reich CI, Reiner DS, Samuelson J, Svard SG, Sogin ML. Genomic minimalism in the early diverging intestinal parasite Giardia lamblia. Science. 2007; 317:1921–1926. [PubMed: 17901334]

12. Marti M, Regos A, Li Y, Schraner EM, Wild P, Muller N, Knopf LG, Hehl AB. An ancestral secretory apparatus in the protozoan parasite Giardia intestinalis. J Biol Chem. 2003; 278:24837–24848. [PubMed: 12711599]
13. Bonifacino JS, Traub LM. Signals for Sorting of Transmembrane Proteins to Endosomes and Lysosomes. Annu Rev Biochem. 2003
14. Boehm M, Bonifacino JS. Genetic analyses of adaptin function from yeast to mammals. Gene. 2002; 286:175–186. [PubMed: 11943473]
15. Nash TE, Aggarwal A, Adam RD, Conrad JT, Merritt JW Jr. Antigenic variation in Giardia lamblia. J Immunol. 1988; 141:636–641. [PubMed: 2454999]
16. Keister DB. Axenic culture of Giardia lamblia in TYI-S-33 medium supplemented with bile. Trans R Soc Trop Med Hyg. 1983; 77:487–488. [PubMed: 6636276]
17. Singer SM, Yee J, Nash TE. Episomal and integrated maintenance of foreign DNA in Giardia lamblia. Mol Biochem Parasitol. 1998; 92:59–69. [PubMed: 9574910]
18. Boucher SE, Gillin FD. Excystation of in vitro-derived Giardia lamblia cysts. Infect Immun. 1990; 58:3516–3522. [PubMed: 2228222]
19. Koradi R, Billeter M, Wuthrich K. MOLMOL: a program for display and analysis of macromolecular structures. J Mol Graph. 1996:14, 51–55. 29–32.
20. Melo F, Feytmans E. Assessing protein structures with a non-local atomic interaction energy. J Mol Biol. 1998; 277:1141–1152. [PubMed: 9571028]
21. Eisenberg D, Luthy R, Bowie JU. VERIFY3D: assessment of protein models with three-dimensional profiles. Methods Enzymol. 1997; 277:396–404. [PubMed: 9379925]
22. Lovell SC, Davis IW, Arendall WB 3rd, de Bakker PI, Word JM, Prisant MG, Richardson JS, Richardson DC. Structure validation by Calpha geometry: phi, psi and Cbeta deviation. Proteins. 2003; 50:437–450. [PubMed: 12557186]
23. Touz MC, Conrad JT, Nash TE. A novel palmitoyl acyl transferase controls surface protein palmitoylation and cytotoxicity in Giardia lamblia. Mol Microbiol. 2005; 58:999–1011. [PubMed: 16262786]
24. Soding J, Biegert A, Lupas AN. The HHpred interactive server for protein homology detection and structure prediction. Nucleic Acids Res. 2005; 33:W244–248. [PubMed: 15980461]
25. Sali A, Potterton L, Yuan F, van Vlijmen H, Karplus M. Evaluation of comparative protein modeling by MODELLER. Proteins. 1995; 23:318–326. [PubMed: 8710825]
26. Slavin I, Saura A, Carranza PG, Touz MC, Nores MJ, Lujan HD. Dephosphorylation of cyst wall proteins by a secreted lysosomal acid phosphatase is essential for excystation of Giardia lamblia. Mol Biochem Parasitol. 2002; 122:95–98. [PubMed: 12076774]
27. Elias EV, Quiroga R, Gottig N, Nakanishi H, Nash TE, Neiman A, Lujan HD. Characterization of SNAREs determines the absence of a typical Golgi apparatus in the ancient eukaryote Giardia lamblia. J Biol Chem. 2008; 283:35996–36010. [PubMed: 18930915]
28. Ullu E, Djikeng A, Shi H, Tschudi C. RNA interference: advances and questions. Philos Trans R Soc Lond B Biol Sci. 2002; 357:65–70. [PubMed: 11839183]
29. Li Z, Kulakova L, Li L, Galkin A, Zhao Z, Nash TE, Mariano PS, Herzberg O, Dunaway-Mariano D. Mechanisms of catalysis and inhibition operative in the arginine deiminase from the human pathogen Giardia lamblia. Bioorg Chem. 2009; 37:149–161. [PubMed: 19640561]
30. Kattenbach WM, Pimenta PF, de Souza W, Pinto da Silva P. Giardia duodenalis: a freeze-fracture, fracture-flip and cytochemistry study. Parasitol Res. 1991; 77:651–658. [PubMed: 1805207]
31. Gaechter V, Schraner E, Wild P, Hehl AB. The single dynamin family protein in the primitive protozoan Giardia lamblia is essential for stage conversion and endocytic transport. Traffic. 2008; 9:57–71. [PubMed: 17892527]
32. Lujan HD, Mowatt MR, Nash TE. Mechanisms of Giardia lamblia differentiation into cysts. Microbiol Mol Biol Rev. 1997; 61:294–304. [PubMed: 9293183]
33. McCaffery JM, Faubert GM, Gillin FD. Giardia lamblia: traffic of a trophozoite variant surface protein and a major cyst wall epitope during growth, encystation, and antigenic switching. Exp Parasitol. 1994; 79:236–249. [PubMed: 7525336]

34. McCaffery JM, Gillin FD. Giardia lamblia: ultrastructural basis of protein transport during growth and encystation. Exp Parasitol. 1994; 79:220–235. [PubMed: 7957746]
35. Faubert G, Reiner DS, Gillin FD. Giardia lamblia: regulation of secretory vesicle formation and loss of ability to reattach during encystation in vitro. Exp Parasitol. 1991; 72:345–354. [PubMed: 2026212]
36. Marti M, Hehl AB. Encystation-specific vesicles in Giardia: a primordial Golgi or just another secretory compartment? Trends Parasitol. 2003; 19:440–446. [PubMed: 14519581]
37. Ullu E, Tschudi C, Chakraborty T. RNA interference in protozoan parasites. Cell Microbiol. 2004; 6:509–519. [PubMed: 15104593]
38. Saraiya AA, Wang CC. snoRNA, a novel precursor of microRNA in Giardia lamblia. PLoS Pathog. 2008; 4:e1000224. [PubMed: 19043559]
39. Prucca CG, Slavin I, Quiroga R, Elias EV, Rivero FD, Saura A, Carranza PG, Lujan HD. Antigenic variation in Giardia lamblia is regulated by RNA interference. Nature. 2008; 456:750–754. [PubMed: 19079052]
40. Lujan HD, Mowatt MR, Helman LJ, Nash TE. Insulin-like growth factors stimulate growth and L-cysteine uptake by the intestinal parasite Giardia lamblia. J Biol Chem. 1994; 269:13069–13072. [PubMed: 8175729]
41. Abodeely M, Dubois KN, Hehl A, Stefanic S, Sajid M, Desouza W, Attias M, Engel JC, Hsieh I, Fetter RD, McKerrow JH. A Contiguous Compartment Functions as Er and Endosome/Lysosome in Giardia Lamblia. Eukaryot Cell. 2009
42. Herz J, Bock HH. Lipoprotein receptors in the nervous system. Annu Rev Biochem. 2002; 71:405–434. [PubMed: 12045102]
43. Knisely JM, Li Y, Griffith JM, Geuze HJ, Schwartz AL, Bu G. Slow endocytosis of the LDL receptor-related protein 1B: implications for a novel cytoplasmic tail conformation. Exp Cell Res. 2007; 313:3298–3307. [PubMed: 17658514]
44. Veniant MM, Zlot CH, Walzem RL, Pierotti V, Driscoll R, Dichek D, Herz J, Young SG. Lipoprotein clearance mechanisms in LDL receptor-deficient “Apo-B48-only” and “Apo-B100-only” mice. J Clin Invest. 1998; 102:1559–1568. [PubMed: 9788969]
45. Yu KC, Chen W, Cooper AD. LDL receptor-related protein mediates cell-surface clustering and hepatic sequestration of chylomicron remnants in LDLR-deficient mice. J Clin Invest. 2001; 107:1387–1394. [PubMed: 11390420]
46. Larkin JM, Donzell WC, Anderson RG. Potassium-dependent assembly of coated pits: new coated pits form as planar clathrin lattices. J Cell Biol. 1986; 103:2619–2627. [PubMed: 2878930]
47. Hernandez Y, Castillo C, Roychowdhury S, Hehl A, Aley SB, Das S. Clathrin-dependent pathways and the cytoskeleton network are involved in ceramide endocytosis by a parasitic protozoan, Giardia lamblia. Int J Parasitol. 2007; 37:21–32. [PubMed: 17087963]
48. Hehl AB, Marti M. Secretory protein trafficking in Giardia intestinalis. Mol Microbiol. 2004; 53:19–28. [PubMed: 15225300]
49. Lanfredi-Rangel A, Attias M, Reiner DS, Gillin FD, De Souza W. Fine structure of the biogenesis of Giardia lamblia encystation secretory vesicles. J Struct Biol. 2003; 143:153–163. [PubMed: 12972352]
50. Conner SD, Schmid SL. Regulated portals of entry into the cell. Nature. 2003; 422:37–44. [PubMed: 12621426]
51. Hashimoto T, Sanchez LB, Shirakura T, Muller M, Hasegawa M. Secondary absence of mitochondria in Giardia lamblia and Trichomonas vaginalis revealed by valyl-tRNA synthetase phylogeny. Proc Natl Acad Sci U S A. 1998; 95:6860–6865. [PubMed: 9618503]
52. Dacks JB, Doolittle WF. Novel syntaxin gene sequences from Giardia, Trypanosoma and algae: implications for the ancient evolution of the eukaryotic endomembrane system. J Cell Sci. 2002; 115:1635–1642. [PubMed: 11950882]

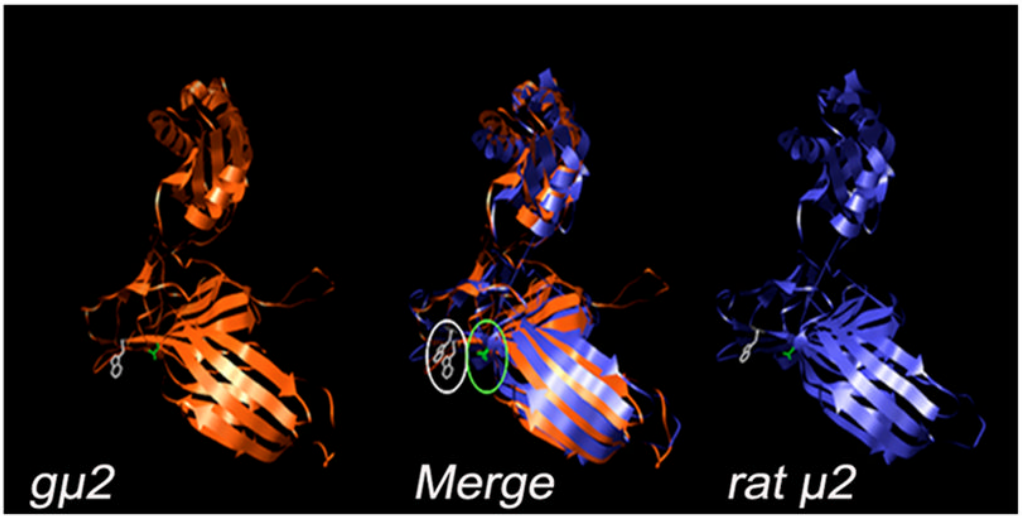

Figure 1. The structure of gμ2 is highly similar to the homologous structure in rat

A 3D reconstruction of gμ2 is compared to the crystallized rat μ2, showing a similar tertiary structure. The substrate-specific binding amino acids Asp^{173} (green) and Trp^{420} (white) are marked.

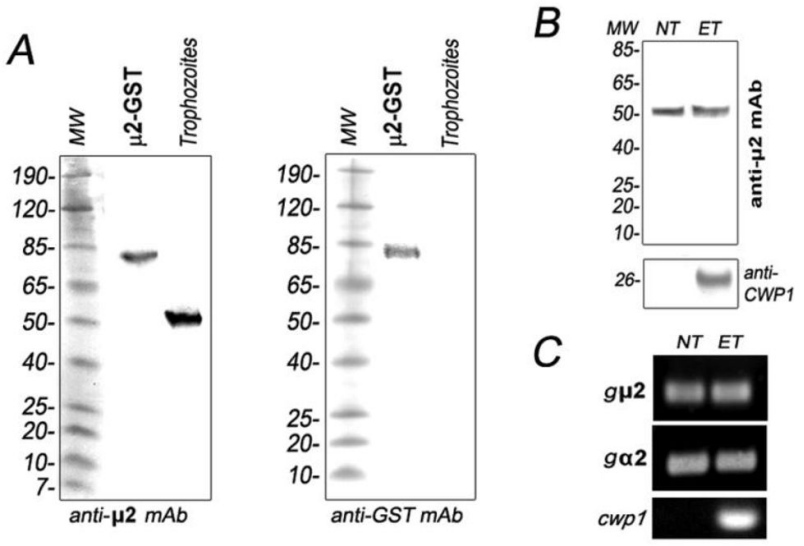

Figure 2. The µ2 subunit of the *Giardia* AP2 complex is equally expressed during cell growth and differentiation

(A) Immunoblotting shows that anti-gµ2 mAb (2F5) detects an 80 kDa band corresponding to the GST-gµ2 fusion protein and a 50 kDa gµ2 protein from trophozoites under reducing conditions (left panel). The anti-GST mAb only detects the GST-gµ2 fusion protein in the same samples as above (right panel). 10 µg of total proteins was added to each well. (B) Immunoblotting evidence shows that the expression of gµ2 in non-encysting trophozoites (NT) is comparable to the encysting ones (ET). CWP1 detection is used as a control for trophozoite encystation. 10 µg of total proteins was added to each well. (C) No variation is observed at the mRNA level by RT-PCR during trophozoite differentiation for both gµ2 and gα2 subunits. mRNA of CWP1 is showed as a control for encystation.

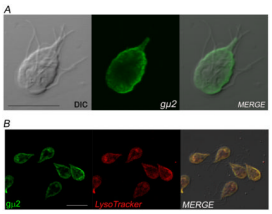

Figure 3. Subcellular distribution of gAP2

(A) IFA and confocal microscopy show that gμ2 localizes predominantly to the peripheral vacuoles (PVs). (B) Live trophozoites were incubated with the lysosomal marker LysoTracker (red), fixed, labelled with anti-gμ2 mAb (green), and analyzed by confocal microscopy. The merged image shows colocalization (yellow) in the PVs. Some cells show colocalization in the bare zone. Bar, 10 μm.

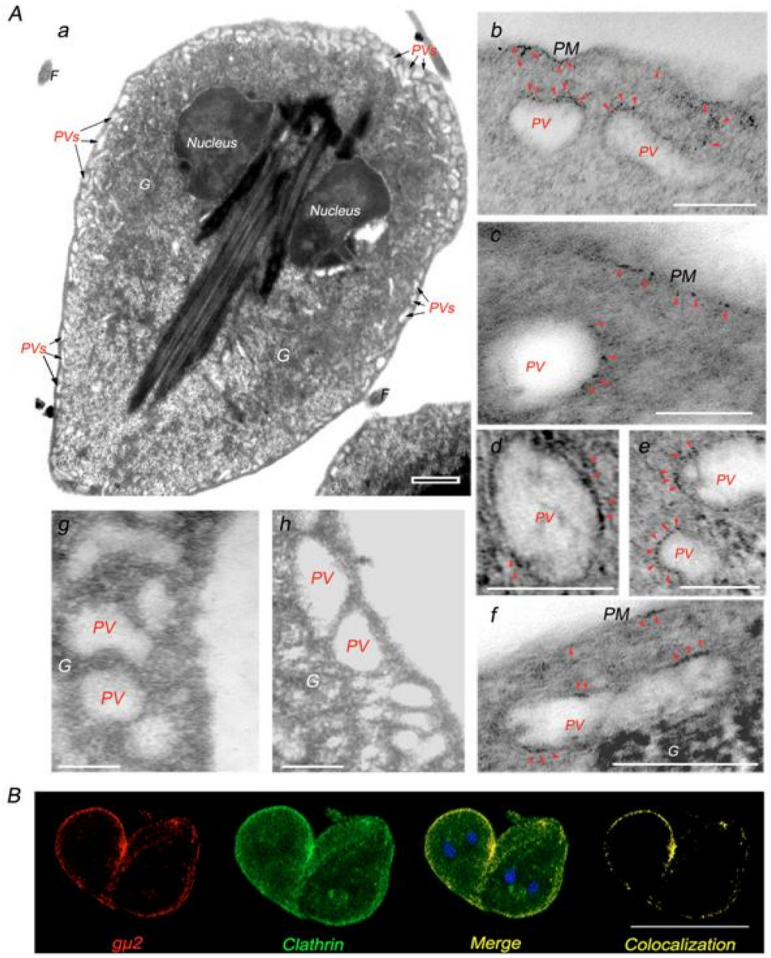

Figure 4. gAP2 localizes to both the lysosome-like peripheral vacuoles and the plasma membrane

(A) (a) Electromicrograph of a growing *Giardia* trophozoite showing the PVs located underneath the plasma membrane (PVs, arrows). Nuclei are also denoted. Bar, 0.5 μm. (b–f) Enlarged immunoelectromicrograph of the PVs. gμ2 (red arrowheads) is detected on the inner side of the plasma membrane and on the PVs. (g) Enlarged electromicrograph of unstained PVs. (h) Electromicrograph of the control using secondary antibody alone. PM: plasma membrane. G: electron-dense glycogen deposits. Bar, 0.1 μm. (B) IFA and confocal microscopy show gμ2 (red) and clathrin (green) in the PV area (Merge-Colocalization). Bar, 10 μm.

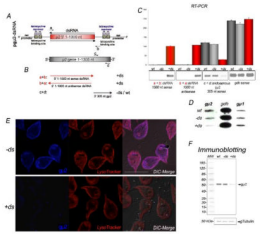

Figure 5. Depletion of gμ2 by long dsRNA production

(A) Schematic representation of the pgμ2-dsRNA vector. After tetracycline induction, the dsRNA is produced under the control of the *Giardia ran* promoters. (B) Graphic of the endogenous gμ2 and the fragments detected by using the **a**, **b**, **c**, and **d** primer combinations. (C) Bars indicates densitometric assessment of one representative RT-PCR experiment. The same amount of 1,000 nt sense and antisense RNA from the vector is observed in +ds trophozoites. Reduction of endogenous *gμ2* mRNA levels is observed in +ds but not in −ds or wild-type cells. Similar expression of *gdh* mRNA in wild-type, −ds and +ds cells is shown. wt: total RNA of wild-type trophozoites. −ds: trophozoites not expressing *gμ2* dsRNA. +ds: trophozoites expressing *gμ2* dsRNA. (D) Two micrograms of total RNA was used for a slot-blot assay. gμ2 depletion is observed only in +ds trophozoites by using the 3′-305-gμ2 antisense. *gdh* and gμ1 antisense probes are shown as controls. (E) Direct IFA and confocal microscopy confirms gμ2 depletion in +ds trophozoites (left bottom panel). LysoTracker staining in −ds and +ds cells is identical. Images were equally processed. Bars, 10 μm. (F) Immunoblotting using anti-gμ2 mAb demonstrates that gμ2 expression is reduced in +ds cells compared with −ds and wild-type (wt) cells (top panel). Uniform tubulin protein expression is observed in the reblotted membrane between wt, −ds, and +ds cells (input control) (bottom panel).

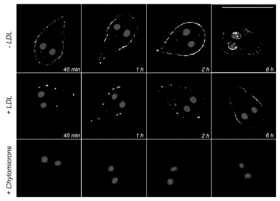

Figure 6. Endocytosis of LDL in *Giardia* trophozoites

Wild-type *Giardia* trophozoites challenged with unlabelled LDL (+LDL panels) show a reduction of BODIPY-LDL uptake compared with unchallenged trophozoites (−LDL). Addition of chylomicrons specifically inhibits the endocytosis of BODIPY-LDL because no fluorescence is observed at any time point in these cells (+Chylomicrons). Bar, 10 μm.

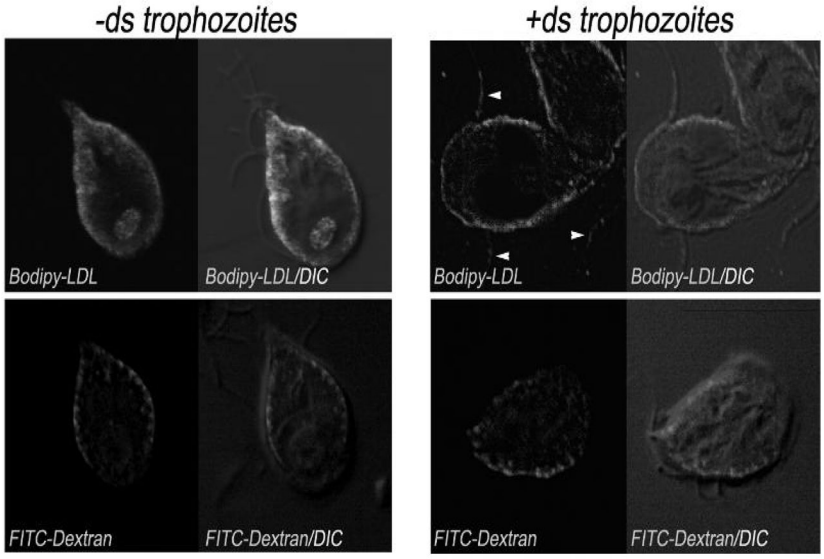

Figure 7. LDL uptake is μ-AP2 mediated

Uptake assays of fluorophore-labelled LDL (BODIPY-LDL) and dextran (FITC-dextran) demonstrate that both the LDL and dextran localize to the PVs in non-permeabilized trophozoite (left panels, −ds). When *gμ2* is depleted, the LDL remains on the surface, including the flagella (arrowheads), while dextran is still internalized to the PVs (right panels, +ds). Bar, 10 μm.

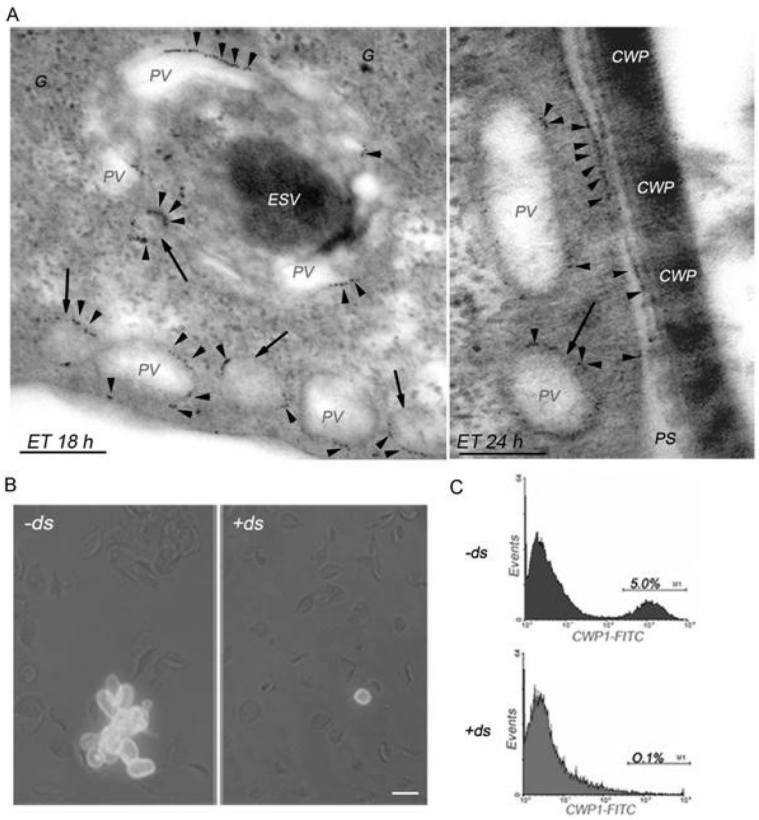

Figure 8. gμ2 plays an essential role during encystations

(A) Enlarged immunoelectromicrograph of encysting WB1267 trophozoites showing PVs surrounding a dense ESV at 18 h post-encystation. gμ2 is primarily observed in the PVs in patches (red arrowheads). At 24 h of encystation, the CWPs are released from the ESVs and assembled, forming the cyst wall. In addition to the PVs, gμ2 is localized on the inner side of the plasma membrane, coincident with the site of electrodense material accumulation outside the cell. Also note electrodense (CWPs) material in some PVs (arrows). Bars, 0.1 μm. G: electron-dense glycogen deposits. PS: periplasmic space. ET: encysting trophozoite. (B) IFA shows mature cysts in −ds cells but not in +ds cells by the detection of CWP1 in the cyst wall (green). Bar, 10 μm. (C) Flow cytometric analysis demonstrating that the positive population represented by the mature cysts (M1) is decreased in +ds (0.1%, bottom panel) compared with −ds cells (5.0%, top panel). One representative experiment of four performed is shown.